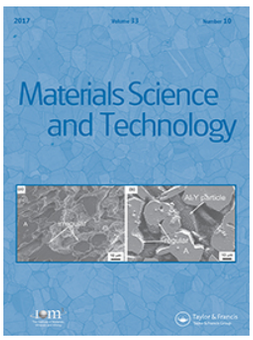

Materials Science and Technology

ISSN: 0267-0836 (Print) 1743-2847 (Online) Journal homepage: https://www.tandfonline.com/loi/ymst20

Microstructure and mechanical behavior of Al9Si0.8Fe alloy with different Mn contents

Renato Baldan, Jefferson Malavazi & Antônio Augusto Couto

To cite this article: Renato Baldan, Jefferson Malavazi & Antônio Augusto Couto (2017) Microstructure and mechanical behavior of Al9Si0.8Fe alloy with different Mn contents, Materials Science and Technology, 33:10, 1192-1199, DOI: 10.1080/02670836.2016.1271966

To link to this article: https://doi.org/10.1080/02670836.2016.1271966

Published online: 12 Jan 2017.

MATERIALS SCIENCE AND TECHNOLOGY, 2017
VOL. 33, NO. 10, 1192–1199
http://dx.doi.org/10.1080/02670836.2016.1271966

The Institute of Materials, Minerals and Mining

Taylor & Francis
Taylor & Francis Group

Microstructure and mechanical behavior of Al9Si0.8Fe alloy with different Mn contents

Renato Baldan[a], Jefferson Malavazi[b] and Antônio Augusto Couto[c]

[a]Campus Experimental de Itapeva, UNESP – Universidade Estadual Paulista, Itapeva, Brazil; [b]Escola SENAI Nadir Dias de Figueiredo, São Paulo, Brazil; [c]IPEN – Instituto de Pesquisas Energéticas e Nucleares, Cidade Universitária, São Paulo, Brazil

ABSTRACT

It has been reported that the detrimental effect of Fe on the mechanical properties of Al alloys can be eliminated through the addition of Mn. In this study, we examine the effects of the addition of different Mn contents (0.1, 0.2, 0.4 and 0.7 wt-% of Mn) on the microstructure and mechanical behaviour of Al9Si0.8Fe alloy. It is shown that the presence of up to 0.4 wt-% of Mn changed the platelike morphology of β-Al_5FeSi into α-$Al_{15}(Fe,Mn)_3Si_2$ with a Chinese script-like morphology. Mn contents higher than 0.4 wt-% promoted the formation of α-$Al_{15}(Fe,Mn)_3Si_2$ phase with a polygonal morphology. The effect of the addition of up to 0.7 wt-% of Mn on the mechanical properties of Al9Si0.8Fe alloys is in fact quite negligible.

ARTICLE HISTORY
Received 9 September 2016
Accepted 9 December 2016

KEYWORDS
Aluminium alloys; intermetallic; iron; manganese; Al9Si0.8Fe

Introduction

Aluminium castings have played an integral role in the growth of the aluminium industry since its inception in the late nineteenth century [1]. Nowadays, Al–Si alloys are among the most popular casting alloys and have a wide range of applications in the automotive and aerospace industries because of their excellent abrasion resistance, low cost, low densities and acceptable mechanical properties [2–4]. In the continuing requirement for automobile weight reduction, the Al–Si alloys have been considered as the promising candidates for bodysheet materials [5].

The microstructure and mechanical properties of Al–Si alloys generally depend on the casting process, composition, solidification rate and heat-treatment. Iron is the most common impurity in aluminium and its alloys. It is not easily removed and it can cause adverse effects on ductility and castability, particularly in the popular Al–Si-based casting alloy [6]. Although iron is highly soluble in liquid aluminium and its alloys, its solubility in the solid state (max. 0.05 wt-%) is very low, so it tends to combine with other elements to form intermetallic phase particles of various types [7,8]. The most common intermetallic phase is β-Al_5FeSi, which forms during solidification and is detrimental to mechanical properties (particularly ductility) because of its brittleness. This deleterious phase also exists in the form of thin plates with edges that act as stress concentration sites, facilitating crack initiation in the matrix [9,10]. Moreover, during the solidification process, these intermetallic particles restrict the flux of interdendritic liquid, leading to the formation of excessive shrinkage defects [3,11].

To counteract the presence of undesirable β-phases, a common practice is to modify the initial chemical composition of the alloy in order to form intermetallic compounds with a more compact morphology [9]. Properly selected chemical elements and compounds, added to alloy in the amounts not changing its chemical composition at a macroscopic scale, can considerably affect its structure (the so-called alloy morphology) and mechanical properties [12].

Some elements (e.g. Cr, Co, Be, Mo and Mn) that cause grain refinement or modify the eutectic silicon phase are added in order to improve the strength/ductility of these alloys and reduce the harmful effect of iron phases [3,13–16]. Additionally, beryllium changes the morphology of Fe-rich intermetallic compounds from needle or platelike to Chinese script or polygons, which is beneficial to the microstructure of the material because fracture initiating sites are mostly located on the coarse β-phase platelets [17,18].

However, one of the most popular modification methods involves the use of chemical elements and compounds, such as Manganese. The purpose of adding Mn is to reduce the detrimental effects of the β-phase by replacing it with the compact and less-detrimental α-$Al_{15}(Fe,Mn)_3Si_2$ phase with polyhedral, star-like and Chinese script morphologies [3,14,15,19]. Microstructural changes other than those produced by the addition of Mn can also be cited: the addition of strontium + manganese in an Al–Si alloy can

CONTACT R. Baldan renatobaldan@gmail.com Campus Experimental de Itapeva, UNESP – Universidade Estadual Paulista, Rua Geraldo Alckmin 519, 18409-010 Itapeva, SP, Brazil

reduce the length of β-Fe thin platelets by 34% [20]; Al–Si–Fe–Cu alloys with manganese contents of up to 0.65 wt-% have shown improved the tensile properties [9]; manganese is also added to increase high-temperature strength and creep resistance through the formation of high-melting compounds [21].

The amount of Mn required to induce the phase transition from β- to α-Fe depends on the cooling rate applied during the solidification of alloy [9,22]. Moreover, the addition of Mn also results in an increase in the total amount of (Fe + Mn)-containing intermetallic compounds in aluminium–silicon alloys [3,19]. Therefore, the addition of Mn is typically restricted to the amount necessary to convert the phase [3]. A common rule to encourage α-Fe phase precipitation is to keep the Mn/Fe ratio at > 0.5 [9,23]. However, the conditions of solidification and/or the presence of other elements in the chemical composition of aluminium–silicon alloys which reduce the effectiveness of Mn (e.g. Cu and Mg) do not completely inhibit the transformation of β-Fe needles into α-Fe Chinese scripts, even at Mn/Fe ratios of up to 2 [24,25].

However, Mn is not always the best solution because it reacts with other elements existing in the melt and forms complex compounds [26]. For instance, Chinese script phase was observed in Mn added Al-9wt-% Si alloy. However, the author remains doubtful on the full transformation of Fe-bearing phases attributed to the Mn addition level at a ratio Mn:Fe = 2:1. Concerning on the effect of Mn on mechanical properties of Al–Si alloys, there is still no a rule of thumb describing the consequence of Mn addition on all Al–Si alloys [27].

Since many commercial aluminium alloys contain manganese and based on the comments above, the aim of this work is to study the effects of the addition of 0.1–0.7 wt-% of Mn on the microstructure and mechanical properties of Al9Si0.8Fe alloy.

Experimental procedure

The chill casting technique was chosen because the cooling rate of the material during solidification is higher than in sand casting. This process promotes a fine-grained microstructure and, consequently, better mechanical properties. The mould was made of H13 steel, as specified by ASTM B108, preheated at 300°C and coated to ensure it would be fully filled and to facilitate the removal of the component. The alloys were produced with pure Al (99.94%), pure Si (98%), Al1.8Fe and Al1.6Mn alloys. Specimens of Al9Si alloy were produced and Al1.8Fe alloy was added to produce the Al9Si0.8Fe alloy, which was used as a reference material for the mechanical tests. Finally, Mn was added to the Al9Si0.8Fe alloy to obtain alloys containing 0.1, 0.2, 0.4 and 0.7 wt-% of Mn.

The material was melted in an induction furnace in a 30 kg crucible and was poured at a temperature of 760°C. The melted alloys were degassed for 5 min in the furnace, using a rotor (300 rev min^{-1} and 15 L min^{-1} of nitrogen) to minimise the formation of oxide particles and hydrogen.

The melted alloys were subjected to a chemical analysis using a GNR Metal Lab 75/80J spectrometer. The as-cast microstructures of each alloy were taken from the cross-section of specimens, prepared using standard metallographic techniques (mounting, grinding, and polishing) and etched with a solution of 0.5% HF. Tensile tests of the as-cast alloys were performed at room temperature (five tests for each alloy) in an EMIC DL 60000 Universal testing machine. The microstructure and fracture surfaces of tensile test specimens were analysed in a scanning electron microscope coupled with an energy dispersive X-ray spectrometer (EDS). The average compositions of the phases were measured using EDS and the results reported here represent an average of approximately five spot analyses.

Results and discussion

Chemical analysis and microstructural characterisation

Table 1 describes the composition of the melted Al9Si0.8Fe alloys with different Mn contents. Note that the Mn content in the alloy is close to the target amount of added Mn.

Figure 1 depicts the microstructure of the Al9Si0.8Fe alloy, showing β-Al_5FeSi and Si particles. Other results regarding the microstructural characterisation of the Al–Si–Fe alloys are reported elsewhere [28].

Figure 2 shows the liquidus projection ternary phase diagram of Al–Si–Fe without Mn (Figure 2(a) and with 0.1 wt-% of Mn (Figure 2(b), adapted from Backerud et al. [29] The addition of Mn changes the fields of the diagram due to the formation of α-$Al_{15}(Fe,Mn)_3Si_2$ phase. Figure 2(b) also shows the solidification path for Al9Si0.8Fe alloy with 0.1 wt-% of Mn. As can be seen, after the formation of α-dendrites from the liquid (A-B field), the following eutectic reactions occur: $L \rightarrow \alpha + \beta$-$Al_5FeSi$ (B-D narrow field), followed by $L \rightarrow \alpha + \alpha$-$Al_{15}(Fe,Mn)_3Si_2$ (D-C field) and finally, the secondary eutectic reaction $L \rightarrow \alpha + Si + \beta$-$Al_5FeSi$ (C field). Figure 3 shows the microstructure of the Al9Si0.8Fe alloy with 0.1 wt-% of Mn. Note the negligible number of small α-$Al_{15}(Fe,Mn)_3Si_2$ particles with Chinese script-like morphology and another platelike intermetallic phase.

Figure 4 shows the liquidus projection ternary phase diagram of Al–Si–Fe with solidification path for the Al9Si0.8Fe alloy containing 0.2 wt-% of Mn, adapted from Backerud et al. [29] A comparison of Figure 2 and 4 indicates that the α-$Al_{15}(Fe,Mn)_3Si_2$ field increases in response to increasing Mn content. The solidification path shows that the formation of the α-dendrites

Table 1. Chemical composition of the melted Al9Si0.8Fe alloys with different Mn contents.

	Al9Si0.8Fe alloy				
Element	Without Mn	0.1 wt-% Mn	0.2 wt-% Mn	0.4 wt-% Mn	0.7 wt-% Mn
Al	89.95 ± 0.08	89.69 ± 0.15	89.50 ± 0.13	89.64 ± 0.09	89.35 ± 0.06
Si	8.99 ± 0.07	8.99 ± 0.10	9.15 ± 0.10	8.75 ± 0.08	8.79 ± 0.06
Fe	0.81 ± 0.01	0.86 ± 0.01	0.87 ± 0.01	0.85 ± 0.01	0.80 ± 0.01
Mn	0	0.12 ± 0.01	0.23 ± 0.01	0.48 ± 0.01	0.73 ± 0.01
Other	0.25	0.34	0.25	0.28	0.33

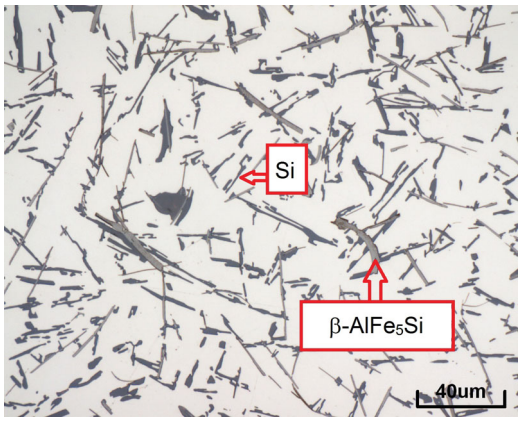

Figure 1. Microstructure of the Al9Si0.8Fe alloy showing β-Al_5FeSi and Si particles.

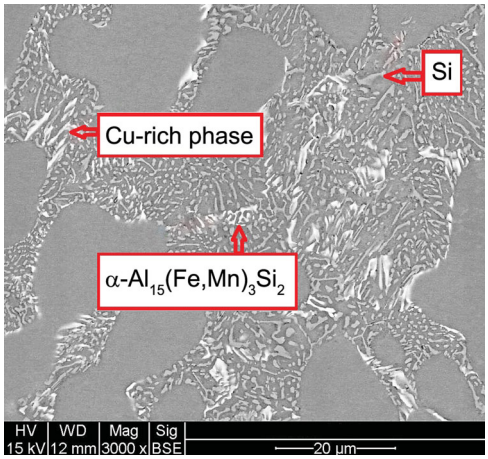

Figure 3. Microstructure of the Al9Si0.8Fe alloy with 0.1 wt-% of Mn.

from the liquid (A-B field) is followed by the eutectic reactions $L \rightarrow \alpha + \alpha\text{-}Al_{15}(Fe,Mn)_3Si_2$ (B-D field), and $L \rightarrow \alpha + Al_5FeSi$ (D-C field) and, finally, by the secondary eutectic reaction $L \rightarrow \alpha + Si + Al_5FeSi$ (C field). Figure 5(a) shows the α-$Al_{15}(Fe,Mn)_3Si_2$ phase with Chinese script-like morphology inside α-Al dendrites of the Al9Si0.8Fe alloy containing 0.2 wt-% of Mn, which were formed by the secondary eutectic reaction, known as coupled eutectic growth. Figure 5(b) depicts β-Al_5FeSi particles with a platelike morphology, α-$Al_{15}(Fe,Mn)_3Si_2$ and Si particles in the microstructure of the alloy.

Figure 6 shows the liquidus projection ternary phase diagram of Al–Si–Fe with the solidification path for Al9Si0.8Fe alloy containing 0.4 wt-% of Mn, adapted from Backerud et al. [29] The solidification path is as follows: eutectic reaction $L \rightarrow \alpha + (\alpha\text{-}Al_{15}(Fe,Mn)_3Si_2)$ (A-B field); $L \rightarrow \alpha + \beta\text{-}Al_5FeSi$ (B-C field); secondary eutectic reaction $L \rightarrow \alpha + Si + Al_5FeSi$ (C field). Additionally, the alloy with 0.4 wt-% of Mn reaches the recommended proportion of 2Fe: 1Mn, which tends to intensify the formation of α-$Al_{15}(Fe,Mn)_3Si_2$. Figure 7 depicts the microstructure of Al9Si0.8Fe alloy containing 0.4 wt-% of Mn. Note the large number of α-$Al_{15}(Fe,Mn)_3Si_2$ particles with Chinese script-like morphology inside the Al dendrites.

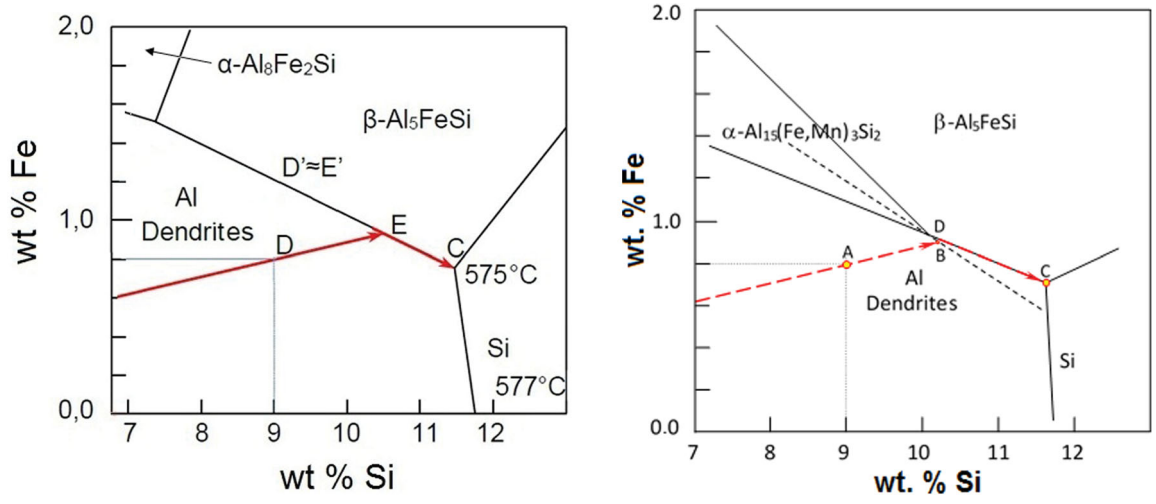

Figure 2. Liquidus projection ternary phase diagram of Al–Si–Fe without Mn (a) and with 0.1 wt-% of Mn (b) showing the solidification path for Al9Si0.8Fe alloy with 0.1 wt-% of Mn. Adapted from Backerud et al. [29].

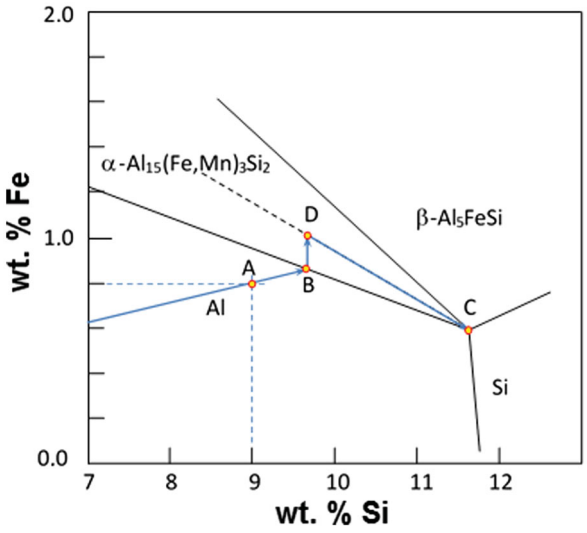

Figure 4. Liquidus projection ternary phase diagram of Al–Si–Fe with solidification path for the Al9Si0.8Fe alloy containing 0.2 wt-% of Mn. Adapted from Backerud et al. [29].

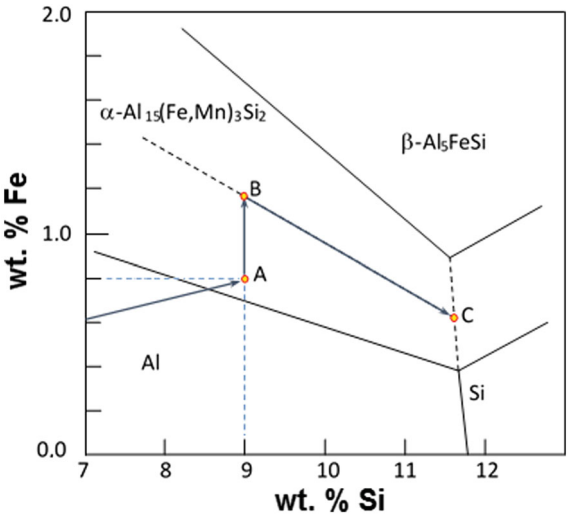

Figure 6. Liquidus projection ternary phase diagram of Al–Si–Fe with the solidification path for Al9Si0.8Fe alloy containing 0.4 wt-% of Mn. Adapted from Backerud et al. [29].

Figure 8(a) shows α-$Al_{15}(Fe,Mn)_3Si_2$ particles with polygonal and Chinese script-like morphologies and Si particles with fibrous morphology in the microstructure of Al9Si0.8Fe alloy containing 0.4 wt-% of Mn. Polygonal particles are formed when the alloy is cooled at high supercooling rates and the Mn content exceeds 0.4 wt-%. Figure 8(b) shows a cross-section of polygonal particles with a polyhedral structure with faceted growing [30,31]. This primary phase emerges before the Al dendrites, which explains its exaggerated growth when compared with Chinese script-like particles formed by coupled eutectic growth [32].

The solidification path of Al9Si0.8Fe alloy containing 0.7 wt-% of Mn was assumed to be the same as that of the alloy with 0.4 wt-% of Mn because it remains within the α-$Al_{15}(Fe,Mn)_3Si_2$ field.

Figure 9(a) shows the formation of a thick polyhedral α-$Al_{15}(Fe,Mn)_3Si_2$ phase in the microstructure of the Al9Si0.8Fe alloy with 0.7 wt-% of Mn, which is attributed to the fact that the Mn content is close to that

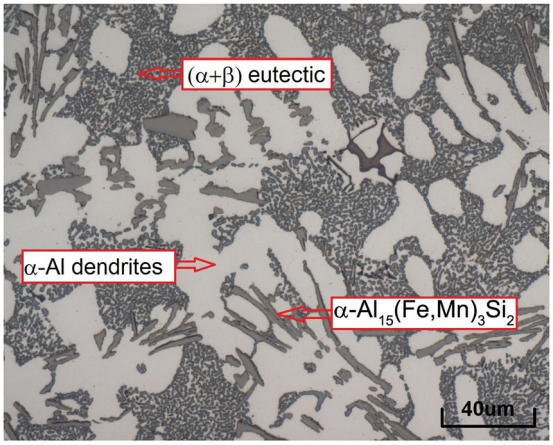

Figure 7. Microstructure of Al9Si0.8Fe alloy containing 0.4 wt-% of Mn.

of Fe in the alloy. In this figure, also note the nucleation and growth of Si particles formed by the secondary eutectic reaction alongside the Mn particles. Finally, according to Figure 9(b), it is important to note that

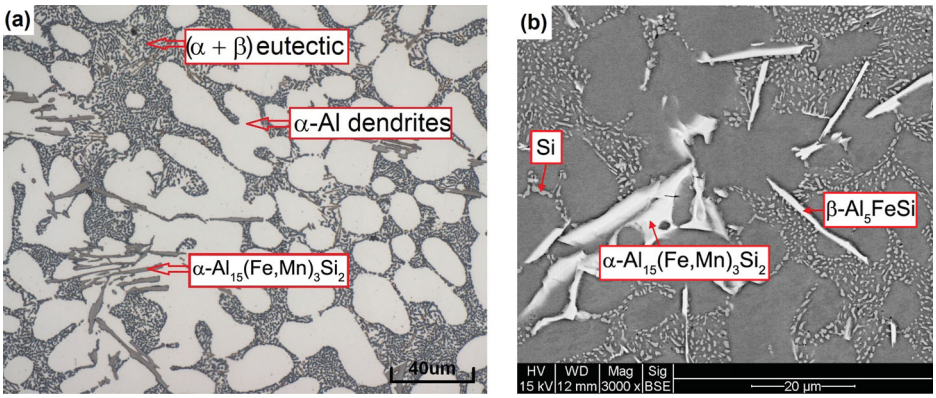

Figure 5. Microstructure of the Al9Si0.8Fe alloy containing 0.2 wt-% of Mn: (a) The intermetallic α-$Al_{15}(Fe,Mn)_3Si_2$ phase with Chinese script-like morphology inside α-Al dendrites; (b) β-Al_5FeSi particles with a platelike morphology, α-$Al_{15}(Fe,Mn)_3Si_2$ and Si particles.

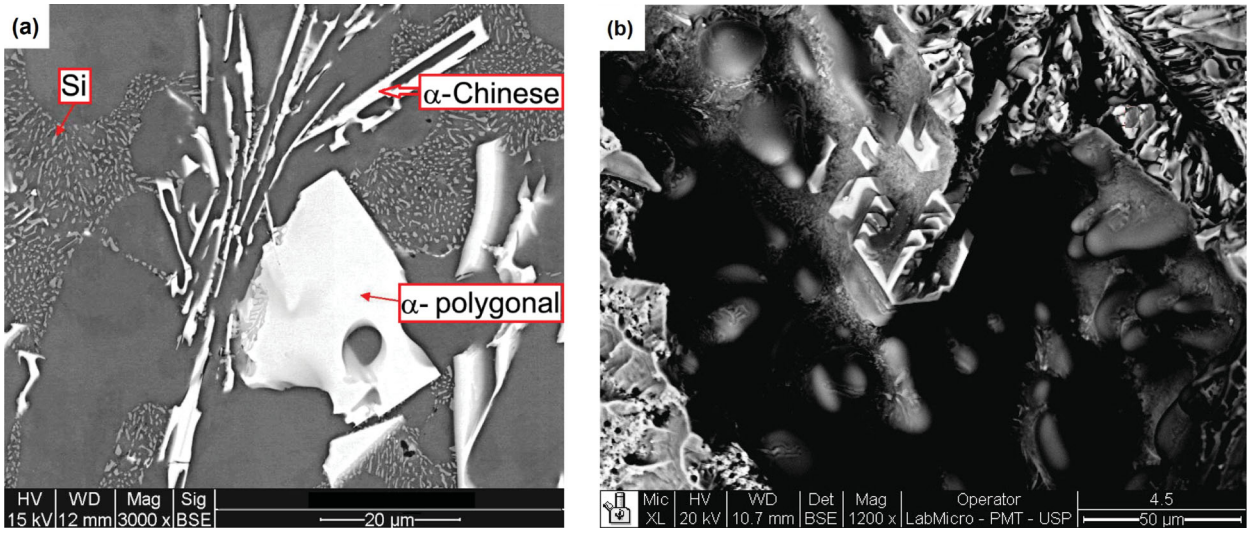

Figure 8. (a) α-$Al_{15}(Fe,Mn)_3Si_2$ particles with polygonal and Chinese script-like morphologies and Si particles with fibrous morphology in the microstructure of Al9Si0.8Fe alloy containing 0.4 wt-% of Mn; (b) cross-section of polygonal α-$Al_{15}(Fe,Mn)_3Si_2$ particles with a polyhedral structure with faceted growing.

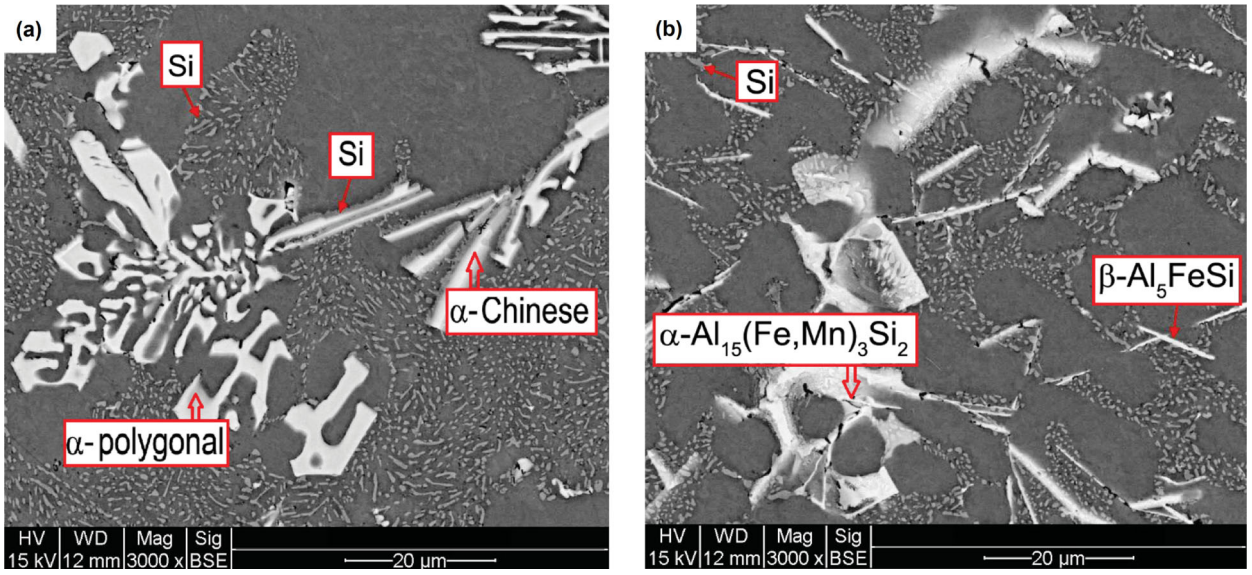

Figure 9. (a) Formation of a thick polyhedral α-$Al_{15}(Fe,Mn)_3Si_2$ phase in the microstructure of the Al9Si0.8Fe alloy containing 0.7 wt-% of Mn; (b) micrograph of the Al9Si0.8Fe alloy containing 0.7 wt-% of Mn showing the presence of the β-Al_5FeSi particles.

higher Mn contents did not prevent the formation of β-Al_5FeSi particles in the alloy's microstructure.

Table 2 shows the EDS analysis of the phases present in the Al9Si0.8 Fe alloy without and with different Mn contents. It is possible to note the presence of copper in the composition of the platelike intermetallic phase of Al9Si0.8 Fe alloy with 0.1 wt-% of Mn. The EDS results of α-$Al_{15}(Fe,Mn)_3Si_2$ phase with polygonal and Chinese script morphologies were also presented.

Mechanical behaviour

Figure 10 shows the tensile test results of the Al9Si0.8Fe alloys. As can be seen, the variations are within the error

Table 2. EDS analysis of the phases present in the Al9Si0.8Fe alloy without and with different Mn contents (α = α-$Al_{15}(Fe,Mn)_3Si_2$; β = β-Al_5FeSi).

	Al9Si0.8 without Mn		Al9Si0.8 Fe0.1Mn			Al9Si0.8 Fe0.2Mn			Al9Si0.8 Fe0.4Mn		Al9Si0.8 Fe0.7Mn	
	Si	β	α	Cu phase	Si	α	β	Si	α-Polygonal	α-Chinese	α-Polygonal	α-Chinese
Oxygen	0.8	11.6	5.0	5.3	1.6	3.0	3.1	2.0	2.2	2.2	4.3	...
Al	10.5	46.9	73.0	70.5	73.9	60.3	55.7	67.9	41.5	43.4	60.5	53.2
Si	88.7	15.0	11.6	10.2	24.5	21.7	24.8	30.1	32.1	30.8	11.7	28.4
Fe	...	26.5	8.3	11.9	...	11.8	13.1	...	17.3	15.2	11.2	10.7
Mn	...	...	2.1	0.7	...	3.2	3.3	...	6.9	8.4	12.3	7.7
Cu	...	...	...	1.4	...	...	...	...	...	...	...	...

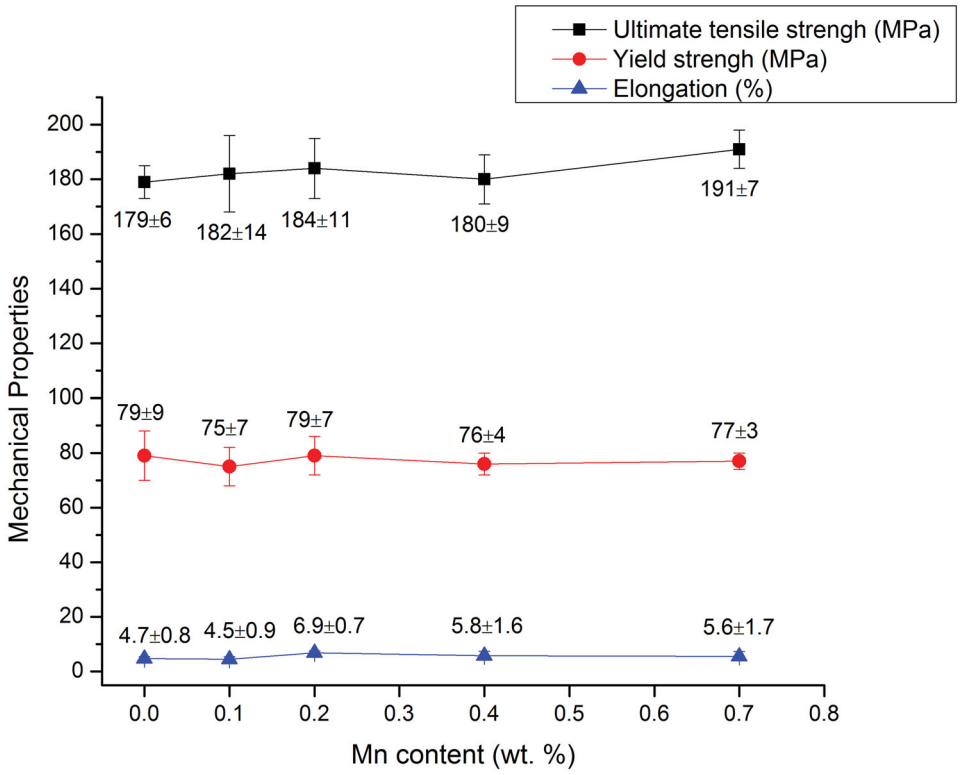

Figure 10. Results of the tensile tests of the Al9Si0.8Fe alloys.

bars, allowing us to conclude that the addition of up to 0.7 wt-% of Mn actually has a negligible effect on the mechanical properties of Al9Si0.8Fe alloys.

The literature reports that while yield strength is not a strong function of Mn content, ultimate tensile strength and elongation increase in response to increased Mn content up to an amount corresponding to a Mn/Fe ratio of ~1.2 [3]. At this Mn/Fe ratio, the platelike β-Al_5FeSi intermetallic phase is completely converted into the Chinese script α-$Al_{13}(Fe,Mn)_4Si_2$ phase. Above this concentration of Mn, the mechanical properties decrease due to the excess amounts of α-phase [3].

Figure 11(a) illustrates the fracture surface of Al9Si0.8Fe alloy containing 0.4 wt-% of Mn. The addition of Mn causes the formation of thick α-$Al_{15}(Fe,Mn)_3Si_2$ particles aligned in the direction of heat-flux extraction. Figure 11(b) shows, in detail, the polyhedral morphology of these precipitates.

Figure 12 depicts the fracture surface of Al9Si0.8Fe alloy with 0.7 wt-% of Mn, showing brittle α-$Al_{15}(Fe,Mn)_3Si_2$ particles with complex morphology surrounded by the ductile α-Al matrix. This combination can improve the mechanical properties of the alloy. The literature reports that fractures initiate and propagate through the interdendritic phases and porosity,

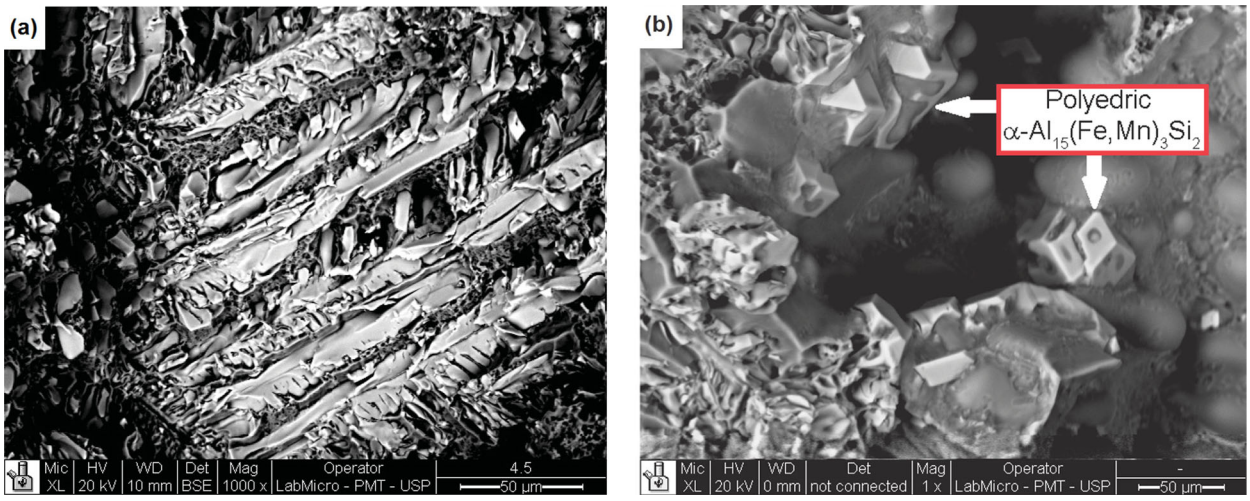

Figure 11. (a) Fracture surface of Al9Si0.8Fe alloy containing 0.4 wt-% of Mn; (b) polyhedral morphology of α-$Al_{15}(Fe,Mn)_3Si_2$ precipitates.

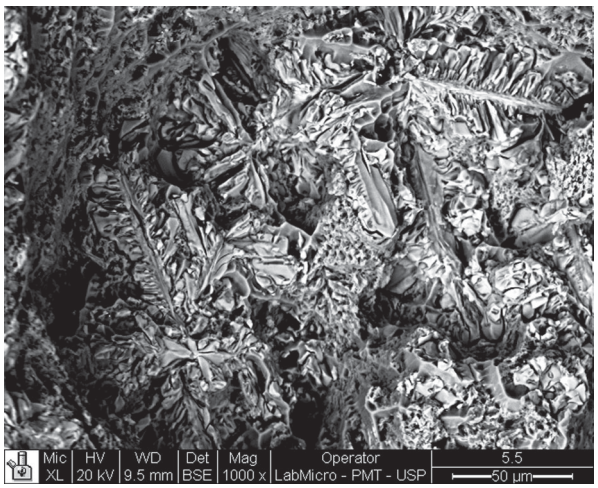

Figure 12. Fracture surface of Al9Si0.8Fe alloy with 0.7 wt-% of Mn.

and that the latter is worse in the alloy with low Mn content due to the inability of the liquid to feed the solidification shrinkage owing to the β-phase platelike morphology [3]. The modification resulting from the addition of Mn to obtain fine well distributed intermetallics may alter the failure mechanism [33]. According to Liu et al. [34], the α-$Al_{15}(Fe,Mn)_3Si_2$ phase can develop to two kinds of morphologies: rhombic dodecahedron and dendrite, in quaternary Al–6Si–4Fe–2Mn alloy under a cooling rate of about 80 K s^{-1}. The different morphologies can be ascribed to the constitutional supercooling effect and cooling rate [34].

Conclusions

The microstructural characterisation and the analysis of the mechanical behaviour of Al9Si0.8Fe alloys with different Mn contents lead to the following conclusions:

- The microstructure of the Al9Si0.8 Fe alloy without Mn showed Si and β-Al_5FeSi particles.
- It was possible to note the negligible number of small α-$Al_{15}(Fe,Mn)_3Si_2$ particles with Chinese script-like morphology and another platelike intermetallic phase in the microstructure of the Al9Si0.8Fe alloy with 0.1 wt-% of Mn.
- The microstructure of Al9Si0.8 Fe alloy containing 0.2 wt-% of Mn showed the α-$Al_{15}(Fe,Mn)_3Si_2$ phase with Chinese script-like morphology inside α-Al dendrites, which were formed by the secondary eutectic reaction, known as coupled eutectic growth, besides β-Al_5FeSi particles with a platelike morphology and Si particles.
- It was possible to note the large number of α-$Al_{15}(Fe,Mn)_3Si_2$ particles with Chinese script-like morphology inside the Al dendrites of Al9Si0.8Fe alloy containing 0.4 wt-% of Mn.
- The microstructure of the Al9Si0.8Fe alloy with 0.7 wt-% of Mn showed the formation of a thick polyhedral α-$Al_{15}(Fe,Mn)_3Si_2$ phase, which is attributed to the fact that the Mn content is close to that of Fe in the alloy.
- Higher Mn contents did not prevent the formation of β-Al_5FeSi particles in the alloy's microstructure.
- The variations in the mechanical properties are within the error bars, leading to the conclusion that the addition of up to 0.7 wt-% of Mn actually exerts only a negligible effect on the mechanical properties of Al9Si0.8Fe alloys.
- The analysis of the fracture surface of the specimens containing 0.4 and 0.7 wt-% of Mn showed α-$Al_{15}(Fe,Mn)_3Si_2$ with polyhedral morphology.
- For future directions, beryllium addition on Al–Si alloys changes the morphology of Fe-rich intermetallic compounds from needle or platelike to Chinese-script or polygons, which is beneficial to the microstructure and mechanical properties of the material.

Disclosure statement

No potential conflict of interest was reported by the authors.

References

[1] Osório WR, Cheung N, Peixoto LC, et al. Corrosion resistance and mechanical properties of an Al 9wt%Si alloy treated by laser surface remelting. Int J Electrochem Sci. 2009;4:820–831.
[2] Li Z, Samuel AM, Samuel FH, et al. Parameters controlling the performance of AA319-type alloys: part I. tensile properties. Mater Sci Eng A. 2004;367:96–110.
[3] Hwang JY, Doty HW, Kaufman MJ. The effects of Mn additions on the microstructure and mechanical properties of Al–Si–Cu casting alloys. Mater Sci Eng A. 2008;488:496–504.
[4] Kang SB, Zhang J, Wang S, et al. Effect of cooling rate on microstructure and mechanical properties in Al–Si alloys. Proceedings of the 12th International Conference on Aluminium Alloys, 2010 Sep 5–9; Yokohama, Japan. The Japan Institute of Light Metals. p. 675–680.
[5] Wang S, Chen S, Matsuda K, et al. Effect of Mn or Fe addition on age-hardening behaviour of $AlMg_2Si$ alloys. Mater Trans. 2012;53:1521–1528.
[6] Taylor JA. Iron-containing intermetallic phases in Al–Si based casting alloys. Procedia Mater Sci. 2012;1:19–33.
[7] Mondolfo LF. Aluminium alloys: structure and properties. 1st ed. London: Butterworths; 1976.
[8] Tang SK, Sritharan T. Morphology of β-AlFeSi intermetallic in AI-7Si alloy castings. Mater Sci Technol. 1998;14:738–748.
[9] Fabrizi A, Ferraro S, Timelli G. The influence of Fe, Mn and Cr additions on the formation of iron-rich intermetallic phases in an Al–Si die-casting alloy. In: Tiryakioglu M, Campbell J, Byczynski G, editors. Shape casting: 5th international symposium 2014. Switzerland: Springer International Publishing; 2014. p. 277–284.
[10] Taghiabadi R, Ghasemi HM. Dry sliding wear behaviour of hypoeutectic Al–Si alloys containing excess iron. Mater Sci Technol. 2009;25:1017–1022.

[11] Han Q, Viswanathan S. Analysis of the mechanism of die soldering in aluminum die casting. Metall Mater Trans A. 2003;34:139–146.
[12] Lipiński T. Tensile strength of the Al-9%Si alloy modified with Na, F and Cl compounds. Arch Foundry Eng. 2010;10:89–92.
[13] Liu L, Samuel FH, Samuel AM, et al. Role of iron in relation to silicon modification in Sr-treated 319 and 356 alloys. Int J Cast Metal Res. 2003;16:397–408.
[14] Narayanan LA, Samuel FH, Gruzleski JE. Crystallization behavior of iron-containing intermetallic compounds in 319 aluminum alloy. Metall Mater Trans A. 1994;25:1761–1773.
[15] Tash M, Samuel FH, Mucciardi F, et al. Effect of metallurgical parameters on the hardness and microstructural characterization of as-cast and heat-treated 356 and 319 aluminum alloys. Mater Sci Eng A. 2007;443:185–201.
[16] Mbuyaa TO, Odera BO, Nganga SP. Influence of iron on castability and properties of aluminium silicon alloys: literature review. Int J Cast Metal Res. 2003;16:451–465.
[17] Nozari M Asadian, Taghiabadi R, Karimzadeh M, et al. Investigation on beneficial effects of beryllium on entrained oxide films, mechanical properties and casting reliability of Fe-rich Al–Si cast alloy. Mater Sci Technol. 2015;31:506–512.
[18] Wang PS, Lee SL, Yang CY, et al. Effect of beryllium and non-equilibrium heat treatment on mechanical properties of B319.0 alloy with 1.0%Fe. Mater Sci Technol. 2004;20:539–545.
[19] Lu L, Dahle AK. Iron-rich intermetallic phases and their role in casting defect formation in hypoeutectic Al—Si alloys. Metall Mater Trans A. 2005;36:819–835.
[20] Malavazi J. Formação dos compostos intermetálicos na liga Al–Si_7 fundida à gravidade. Fundição e Matérias-Primas. 2012;1:78–91.
[21] Shabestari SG. The effect of iron and manganese on the formation of intermetallic compounds in aluminum–silicon alloys. Mater Sci Eng A. 2004;383:289–298. doi:10.1016/S0921-5093(04)00832-9.
[22] Belmares-Perales S, Castro-Román M, Herrera-Trejo M, et al. Effect of cooling rate and Fe/Mn weight ratio on volume fractions of α-AlFeSi and β-AlFeSi phases in Al–7.3Si–3.5Cu alloy. Met Mater Int. 2008;14:307–314.
[23] Ji S, Yang W, Gao F, et al. Effect of iron on the microstructure and mechanical property of Al–Mg–Si–Mn and Al–Mg–Si die cast alloys. Mater Sci Eng A. 2013;564:130–139.
[24] Seifeddine S, Johansson S, Svensson IL. The influence of cooling rate and manganese content on the β-Al5FeSi phase formation and mechanical properties of Al–Si-based alloys. Mater Sci Eng A. 2008;490:385–390.
[25] Khalifa W, Samuel AM, Samuel FH, et al. Metallographic observations of β-AlFeSi phase and its role in porosity formation in Al-7%Si alloys. Int J Cast Metal Res. 2006;19:156–166.
[26] Ashtari P, Tezuka H, Sato T. Influence of Sr and Mn additions on intermetallic compound morphologies in Al–Si–Cu–Fe cast alloys. Mater Trans. 2003;44:2611–2616.
[27] Ervina Efzana MN, Kong HJ, Kok CK. Review: effect of alloying element on Al–Si alloys. Adv Mater Res. 2013;845:355–359.
[28] Malavazi J, Baldan R, Couto AA. Microstructure and mechanical behaviour of Al9Si alloy with different Fe contents. Mater Sci Technol. 2015;31:737–744.
[29] Backerud L, Chai G, Tamminen J. Solidification characteristics of aluminum alloys. Vol. 2. Oslo, Norway: Foundry Alloys, AFS/ScanAluminium; 1990. p. 81–82.
[30] Roy N, Samuel AM, Samuel FH. Porosity formation in Al-9 wt pct Si-3 wt pct Cu alloy systems: metallography observations. Metall Mater Trans A. 1996;27:415–429.
[31] Jarstad JL. Understanding Sludge. Proceedings of the 14th SDCE International Die Casting Congress and Exposition; 1987 May 11–14; Toronto, Ontario, Paper No. G-T87-011.
[32] Dinnis CM, Taylor JA, Dahle AK. As-cast morphology of iron-intermetallics in Al–Si foundry alloys. Scripta Mater. 2005;53:955–958.
[33] Emamy M, Abedi K. The effect of Fe, Mn and Sr on the microstructure and tensile properties of A356–10%SiC composite. Mater Sci Eng A. 2010;527:3733–3740.
[34] Liu X, Li C, Wu Y, et al. Morphologies and growth mechanisms of α-Al(FeMn)Si in Al–Si–Fe–Mn alloy. Mater Lett. 2013;110:191–194.